Corrosion behavior of TaC coated AZ31 Alloy

A. Danalakshmi[1,2] and A. Cyril[2]
[1,2]*Research Scholar, Department of Industrial Chemistry,*
Alagappa University, Karaikudi, Sivaganga (Tamilnadu), India.
[2]*Assistant Professor Post graduate & Research Department of Chemistry,*
Raja Dorasingam Government Arts College, Sivaganga (Tamilnadu), India.

(Corresponding author: A. Cyril)

ABSTRACT: In this work, the tantalum carbide coating was developed on AZ31 alloy by physical vapor deposition technique. The TaC-coated AZ31 alloy phase purity and crystallinity were examined using X-ray diffraction analysis. The surface morphology of TaC coatings on AZ31 alloy was analyzed using scanning electron microscope (SEM). The chemical speciation and oxidation states of the elements are determined by X-ray photoelectron spectroscopy (XPS) technique. The corrosion characteristics of TaC coating over AZ31 are examined in 3.5 % NaCl electrolyte using three electrode based electrochemical cell. The bare AZ31 alloy shows the corrosion potential of -1.45 V (SCE) and corrosion current density of 3.2×10^{-4} mA/cm^2. The TaC coated AZ31 demonstrated -1.18 V (SCE) corrosion potential and 5.36×10^{-6} mA/cm^2 corrosion current density. The noble shift in the potential for the AZ31 alloy is really challenging and it is attained due to the TaC coatings. The results reveal that the TaC coated AZ31 alloy demonstrated higher corrosion resistance than the bare AZ31.

I. INTRODUCTION

As the magnesium metal and its alloys suffer high corrosion rates due to its high negative potential in electromotive force, and hence, mostly their applications in various fields are restricted. However, recent developments on finding the surface treatments either by inhibitors or surface coatings on magnesium alloys pave newer pathways for the applications. The application of corrosion inhibitors is an effective tool to lower the metal or alloy corrosion dissolutions [1-5]. The electrostatic interactions, these inhibitors form a protective film over the surface and provide lower corrosion rates [1-5]. Mostly, high metallic salts and heterocycles applied as corrosion inhibitors for Mg alloys [6-9]. Due to their high toxicity, the production of these inhibitors has some limitations or restrictions. Ma *et al.,* (2011) studied the effect of chromate addition on the corrosion rate of magnesium alloys and demonstrated the $MgCr_2O_4$ spinel structure formed on the surface of AZ91D alloy and demonstrated higher corrosion protections [6]. Wu *et al.,* (2010) fabricated diamond like DLC/AlN/Al coating on AZ31 using magnetron sputtering method. In 3.5 % NaCl electrolyte, the authors demonstrated -1.47 V corrosion potential (SCE) and proposed that a tri-layered coatings consists of DLC/AlN/Al shows positive or noble shift in corrosion potential for AZ31 [10]. Han *et al.,* (2017) developed graphene based coatings on AZ31 alloy using anodizing oxidation technique. The corrosion resistance of graphene based anodic coating on AZ31 demonstrated that the corrosion potential shifted to more noble side with increase in the graphene concentration. The authors also demonstrated the -1.15 V (SCE) in 3.5 % NaCl electrolyte [11]. Yaowei *et al.,* (2017) developed tugsten carbide coatings on AZ31 by plasma electrolytic oxidation method and demonstrated the corrosion potential -1.3 V (SCE) in 3.5 % NaCl electrolyte [12].

In this work, the tantalum carbide coating developed on AZ31 alloy by physical vapor deposition technique. The TaC-coated AZ31 alloy phase purity and crystallinity examined using X-ray diffraction analysis. The surface morphology of TaC coatings on AZ31 alloy analyzed using scanning electron microscope (SEM). The chemical speciation and oxidation states of the elements are determined by X-ray photoelectron spectroscopy (XPS) technique. The corrosion characteristics of TaC coating over AZ31 are examined in 3.5 % NaCl electrolyte using three electrode based electrochemical potentiostat. The results reveal that the corrosion potential is -1.18 V (SCE) with higher corrosion resistance.

II. MATERIALS AND METHODS

Chemicals: Tantalum carbide sputtering target was purchased from Stanford advanced materials (USA) with 99.9 % purity.

TaC coatings development: For the TaC, the deposition temperature was in the range between 70 and 420ºC. Prior to the coating deposition a thin (~ 0.1 μm) Ti intermediate layer was deposited to improve adhesion of the coatings. The TaC coating was developed with 10-20 μm.

Sample preparation: The sample with 12 × 12 × 6 mm dimensions were cut from sheet and polished from 200 to 1200 SiC grit paper and mirror polished using 0.5 μm diamond paste embedded cloth using metallurgical polishing machine.

Electrochemical experiments: A three electrode system was used for analyzing the open circuit potentials; Tafel plots to determine corrosion current densities and electrochemical impedance spectroscopy.

The AZ31 specimens as working electrode, saturated calomel (SCE) as reference electrode and platinum foil as counter electrode.

III. RESULTS AND DISCUSSION

X-ray diffraction analysis: The phase purity and crystallinity of TaC coated AZ31 sample was characterized by X-ray diffraction analysis and the XRD pattern is shown in Fig. 1. The bare AZ31 alloy exhibit sharp peaks, which are well matched to standard JCPDS file no # 35-0821. The peaks and the corresponding planes indicate that the hexagonal crystal structure with a space group of P63/mmc for Mg alloy. The crystal lattice parameters are a=b=3.2094 Å and c=5.211Å. The planes which are marked in red color (111), (200) and (220) are corresponds to the cubic phase of TaC coating, where a=b=c=4.4460 Å and belongs Fm3m space group. From the Fig. 1 is noticed that the (111) plane demonstrated highest intensity shows and confirms the presence of TaC coating over AZ31 alloy.
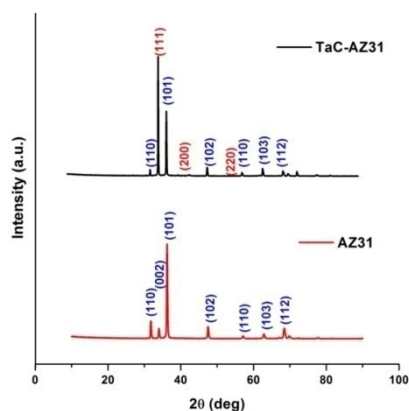

Fig. 1. X-ray diffraction pattern of bare and TaC coated AZ31 alloy.

Yaowei *et al.*, (2017) developed WC/TaC reinforced Nickel-Based Composite Alloy Coating by Laser Cladding and showed the (111) plane is major peak for TaC compound. The obtained and presented peaks in this work for TaC are well matched with the literature [12].

SEM Analysis: The surface morphology and elemental composition of TaC coated AZ31 alloy are examined using scanning electron microscope (SEM). The surface morphology of bare AZ31 alloy is presented in Fig. 2.
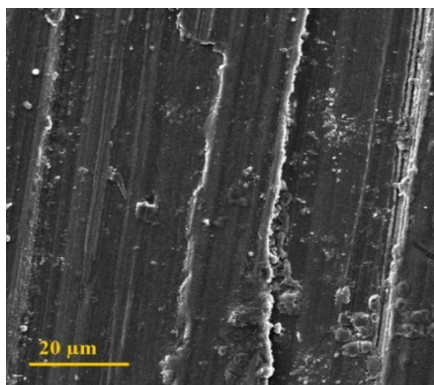

Fig. 2. Surface morphology of TaC coated AZ31 alloy.

The surface morphologies of TaC coated AZ31 alloy at various locations are shown in Figs. 3 (a-c).
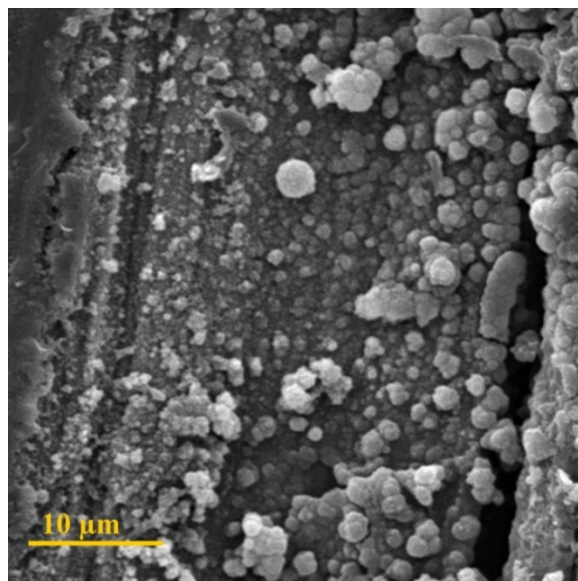

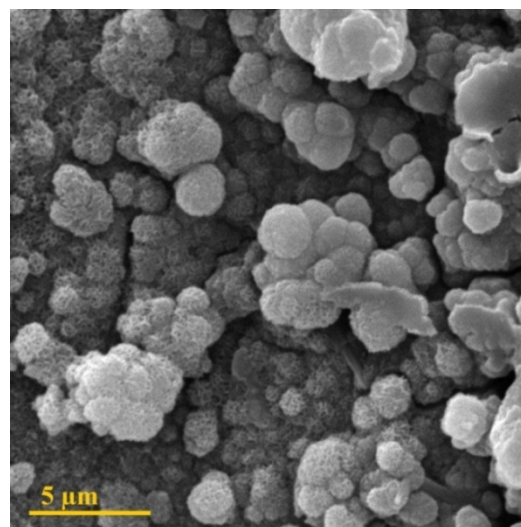**Fig. 3.** (a) Surface morphology of TaC coated AZ31 alloy.

Fig. 3. (b) Surface morphology of TaC coated AZ31 alloy.

Figs. 3 (a-c) demonstrates the surface is enriched with meso-porous spherical particles deposited on AZ31 alloy. The particles consists of nanoflakes within the micron sized spherical shape particles. Kumar *et al.*, (2017) fabricated TaC/SiC coatings over graphite and demonstrated spherical shape morphology for TaC coating, which is developed by chemical vapour deposition technique. The authors also obtained micron size spherical morphology [13]. Nakamura *et al.*, (2017) developed TaC coatings using the chemical vapor deposition technique and demonstrated that initially spherical particles were formed consisting TaC with various porosity and after annealing the surface of coatings changed to highly dense with lower porosity [14]. The obtained morphology in the present work also matches with reported literature.
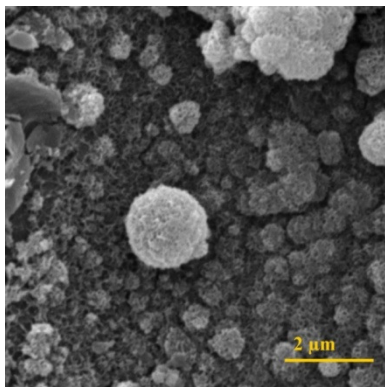
Fig. 3. (c) Surface morphology of TaC coated AZ31 alloy.

XPS analysis: Surface chemical valance states of various elements in the TaC-AZ31 alloy are examined X-ray photoelectron spectroscopy (XPS) technique.
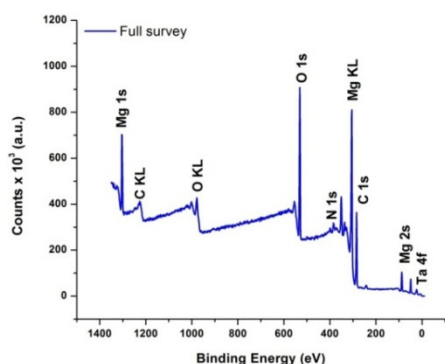

Fig. 4. XPS full survey spectrum for TaC coated AZ31 alloy.

The full survey spectrum of TaC coated AZ31 alloy is shown in Fig. 4. The spectrum shows the presence of Ta 4f, Mg1s, C1s and O1s elements with respective KLL peaks. The high resolution spectrum of Mg1s is presented in Fig. 5. The peaks are deconvulated using Shirley fit.
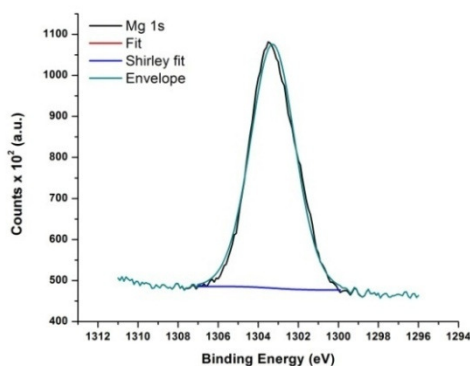

Fig. 5. XPS Mg1s spectrum of TaC coated AZ31 alloy.

Mg 1s spectrum is decomposed into single peak with the binding energy of 1303 eV, which indicates elemental Mg with zero state. The curve is seen that symmetric in nature. The overlapping ambiguity with Ca2p and Cl LMM, is eliminated with the presence of Mg KLL peak at 300 eV. In the full survey spectra, Mg 2s peak also presented and affirms the presence of Mg

in AZ31 alloy. For the coating of TaC, the C1s element high resolution spectrum also recorded and presented in Fig. 6. The C1s spectrum is deconvulated into three peaks with the binding energies of 284.3 eV, 287.1 eV and 288 eV. The binding energy at 284.3 represents the metallic carbon, which is used for all the binding energy calibration. The peak at 287.1 eV corresponds to Ta-C bond and the last one at 288 eV shows the O-C=C bonds. The latter might have attained from organic contamination. Since, XPS is surface sensitive, these peaks are un-avoidable. However, the C1s spectrum confirms the presence of metallic carbide, which is bound to Ta.
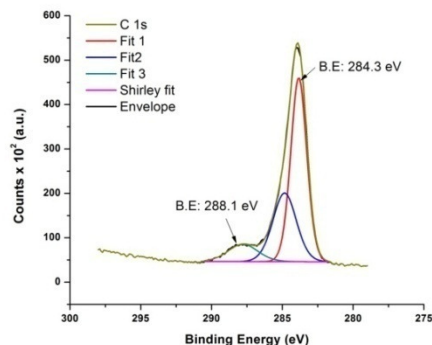

Fig. 6. XPS spectrum of C1s of TaC coated AZ31 alloy.

The high resolution Al 3p spectrum is shown in Fig. 7. The spectrum is decomposed into single peak with the binding energy of 73 eV, which indicate that the metallic Al. The high resolution spectrum for Zn is not provided due the weak signals obtained from lower composition the element.
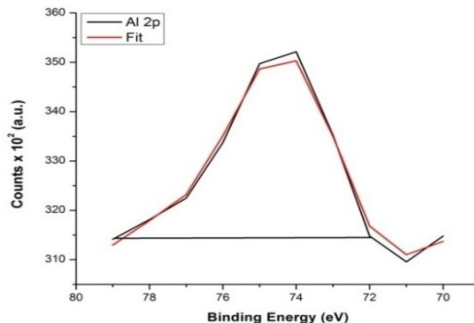

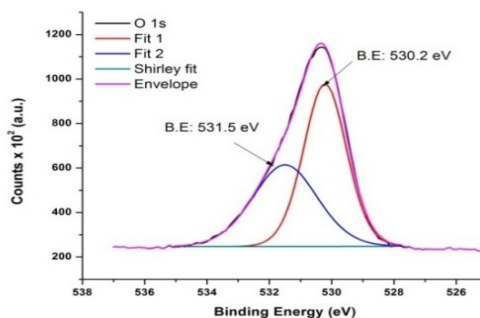**Fig. 7.** XPS spectrum of Al 2p of TaC coated AZ31 alloy.

Fig. 8. XPS spectrum of O1s of TaC coated AZ31 alloy.

The high resolution spectrum of O1s is shown in Fig. 8. The O1s spectrum is decomposed into two peaks at

530.2 eV and 531.5 eV. The peak at 530.2 eV represents the metallic oxides and the peak at 531.5 eV indicates the metal hydroxides. These peaks attributed to the surface contamination and chemical reactivity of Mg alloy with oxygen and CO_2 during the sample storage and transpiration into the XPS analysis chamber. All the binding energies were calibrated against C1s spectrum, which is shown in Fig. 6. The high resolution Ta4f spectrum is shown in Fig. 9. The Ta 4f spectrum is deconvulated into three peaks.
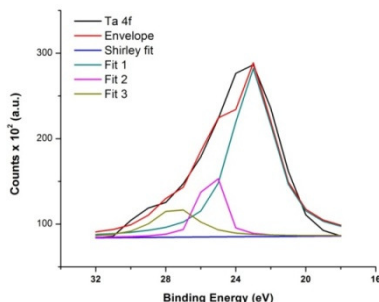

Fig. 9. XPS spectrum of Ta 4f of TaC coated AZ31 alloy.

The peak at 23.4 eV represents the metallic tantalum. The peak at 25.3 eV and 27.8 eV are corresponds to oxidized tantalum. During physical vapor deposition, the oxygen percentage maintained as low as possible, however, the oxygen entraps into the systems and show reactivity with metals. This might be reason for the presence of oxidized tantalum. Behera *et al.*, (2017) also demonstrated the presence these oxidized peaks at reported binding energies in this work [15].

Raman analysis: Raman spectrum of TaC coating is shown in Fig. 10. The disordered peak at 1350 cm^{-1} and the graphite peak at 1580 cm^{-1} are attained from TaC and C. the same behavior also observed by Kim *et al.*, (2016) reported work [16].

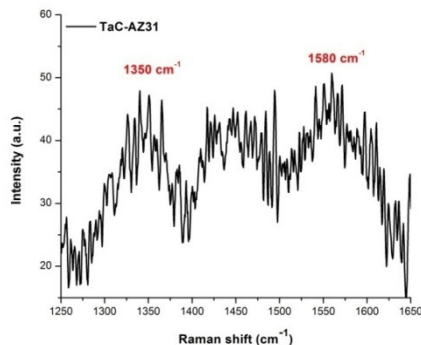
Fig. 10. Raman spectrum of TaC coated AZ31 alloy.

Electrochemical polarization analysis:
Electrochemical polarization analysis: The schematic representation of three electrode system is shown in Fig. 11. A three electrode assembly was used for analyzing the polarization experiments to collect the corrosion data of the specimen and electrochemical impedance spectroscopy. The TaC coated AZ31 specimen as working electrode, saturated calomel (SCE) as reference electrode and platinum foil as counter electrode. The electrolyte of 3.5 % NaCl was employed in the present work.
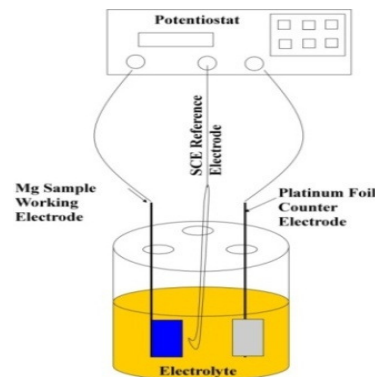

Fig. 11. Schematic representation of three electrode electrochemical cell.

The TaC coated AZ31 electrical connections were made using copper wire as shown in Fig. 11. Only polished surface is exposed to the electrolyte and other faces are masked with insulating organic coating. Before commencing the experiment, electrical contact is tested for all the electrodes.

Fig. 12. The TaC coated AZ31 alloy electrode.

The Tafel plot of AZ31 alloy without coating is shown in Fig. 13. The cathodic reaction is generally hydrogen evolution during cathodic scan shown in Tafel plot. In anodic region, the curve proceeds vertically, signifying the formation protective film over the surface AZ31 alloy. The noise in anodic curve is attributed to the failure of passive film due to the attack of Cl⁻ ions [17]. Similarly, the electrochemical impedance spectrum is shown in Fig. 14. The liner polarization curve of TaC coated AZ31 is shown in Fig. 15 and the corresponding impedance spectrum is shown in Fig. 16.
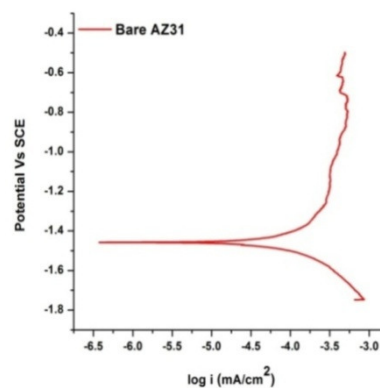

Fig. 13. Linear polarization curve of bare AZ31 in 3.5 % NaCl solution.
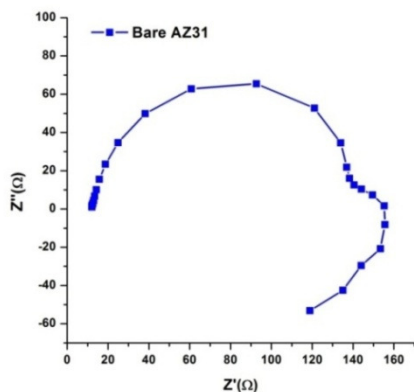
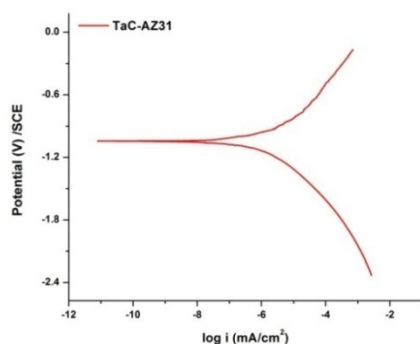**Fig. 14.** Electrochemical impedance spectrum of bare AZ31 in 3.5 % NaCl solution.

Fig. 15. Linear polarization curve of TaC coated AZ31 alloy in 3.5 % NaCl solution.
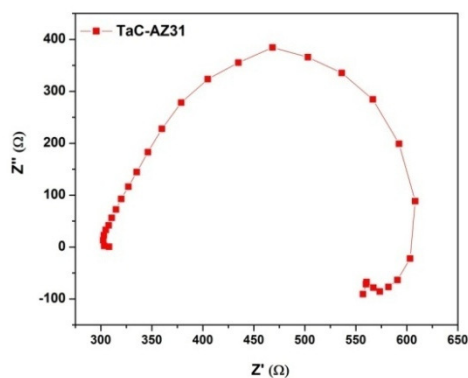

Fig. 16. Electrochemical impedance spectrum of TaC coated AZ31 in 3.5 % NaCl solution.

The Figs. 13&15 indicate the potentiodynamic linear polarization curves of bare AZ31 and TaC coated AZ31 in 3.5 % NaCl solutions. It is seen that the bare AZ31 show the corrosion potential at -1.45 V (SCE), where as the TaC coated AZ31 alloy shows -1.13 V (SCE) From this, it is noticed that TaC coated AZ31 shows higher corrosion resistance than bare AZ31. The electrochemical impedance spectra of bare AZ31 and TaC coated AZ31 in 3.5 % NaCl solutions. It is seen that the radius of conductive loop of bare AZ31 show lower and the radius of conductive loop for TaC coated AZ31 shows highest, which indicate that TaC coated AZ31 shows better corrosion resistance property for AZ31 alloy in 3.5 % NaCl solutions.

The surface morphology of the TaC coated AZ31 after corrosion is shown in Fig. 17 and 18. The surface morphology is completely changes after corrosion. More pits and corrosion products are noticed. The high chemical reactivity of magnesium alloys in chloride environment of AZ31 alloy.
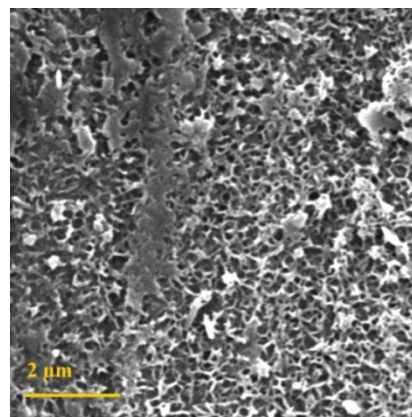

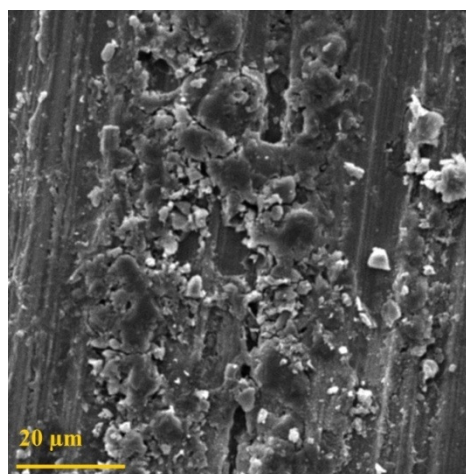**Fig. 17.** Surface morphology of TaC coated AZ31 after corrosion in NaCl solution

Fig. 18. Surface morphology of TaC coated AZ31 after corrosion in NaCl solution.

IV. CONCLUSION

The tantalum carbide coating was developed on AZ31 alloy by physical vapor deposition technique. The TaC-coated AZ31 alloy phase purity and crystallinity examined using X-ray diffraction analysis. The surface morphology of TaC coatings on AZ31 alloy analyzed using scanning electron microscope (SEM). The chemical speciation and oxidation states of the elements are determined by X-ray photoelectron spectroscopy (XPS) technique. The corrosion characteristics of TaC coating over AZ31 are examined in 3.5% NaCl electrolyte using three electrode based electrochemical cell. The bare AZ31 alloy shows the corrosion potential of -1.45 V (SCE) and corrosion current density of 3.2×10^{-4} mA/cm^2. The TaC coated AZ31 demonstrated -1.18 V (SCE) corrosion potential and 5.36×10^{-6} mA/cm^2 corrosion current density. The results reveal that the TaC coated AZ31 alloy demonstrated higher corrosion resistance than the bare AZ31.

V. FUTURE SCOPE

The TaC coating fabricated by vapor deposition improves the corrosion resistance of AZ31 alloy. Using this method, the corrosion resistance can be improved the magnesium alloy parts, which are currently being used in actual applications in automobile and aerospace applications. The proposed methods can applied for scale up technologies for magnesium alloys. The research can be focused in these directions for the enhanced corrosion resistance of other magnesium alloys.

Conflict of Interest. No conflict of interest.

REFERENCES

[1]. Sorkhabi, H. A., Seifzadeh, D., & Hosseini M. G. (2008). EIS and polarization studies to evaluate the inhibition effect of 3H-phenothiazin-3-one, 7-dimethylamin on mild steel corrosion in 1M HCl solution, *Corros. Sci. 50*, 3363–3370.

[2]. Ashassi-Sorkhabi, H., & Seifzadeh, D. (2008). Analysis of raw and trend removed EN data in time domain to evaluate corrosion inhibition effects of New Fuchsin dye on steel corrosion and comparison of results, *J. Appl. Electrochem*, *38*, 1545–1552.

[3]. Khaled, K. F. (2010). Experimental, density function theory calculations and molecular dynamics simulations to investigate the adsorption of some thiourea derivatives on iron surface in nitric acid solutions, *Appl. Surf. Sci*. Vol. *256*, 6753–6763.

[4]. Li, C., Li, L., & Wang, C. (2014). Study of the inhibitive effect of mixed self-assembled monolayers on copper with SECM, *Electrochim. Acta*, *115*, 531–536.

[5]. Mobin, M., Parveen, M., & Rafiquee, M. Z. A. (2013). Synergistic effect of sodium dodecylsulfate and cetyltrimethyl ammonium bromide on the corrosion inhibition behavior of l-methionine on mild steel in acidic medium, *Arab J. Chem*. 24, 81–99.

[6]. Ma, Y., Liu, N., Wang, Y. S., Wang, J. S., & Guo, H. X. (2011). Effect of chromate additive on corrosion resistance of MAO coatings on magnesium alloys, *J. Chin. Ceram. Soc*., *39*, 1493-1497.

[7]. Liu, Y.L., Yong, Z.Y., Zhou, S.X., & Wu, L.M., (2008). Molybdate/phosphate composite conversion coating on magnesium alloy surface for corrosion protection, *Appl. Surf. Sci*., *255*, 1672-1680.

[8]. Gao, H., Li, Q., Dai, Y., Luo, F., & Zhang, H.X., (2010). High efficiency corrosion inhibitor 8-hydroxyquinoline and its synergistic effect with sodium dodecylbenzenesulphonate on AZ91D magnesium alloy, *Corros. Sci*., *52*, 1603–1609.

[9]. Seifzadeh, D., Bezaatpour, A., & Asadpour Joghani, R. (2014). Corrosion inhibition effect of N, N′-bis (2-pyridylmethylidene)- 1, 2-diiminoethane on AZ91D magnesium alloy in acidic media, *Trans. Nonferrous Met. Soc. China. 24*, 3441–3451.

[10]. Wu, G., Dai, W., Zheng, H., & Wang, A. (2010). Improving wear resistance and corrosion resistance of AZ31 magnesium alloy by DLC/AlN/Al coating. *Surface and Coatings Technology, 205*(7), 2067–2073

[11]. Han, B. (2017). A Composite Anodic Coating Containing Graphene on AZ31 Magnesium Alloy.*International Journal of Electrochemical Science,* 9829–9843.

[12]. Yaowei, Y., Wei, F., Xiang, Z., Qilin, D., & Jianguo, Y. (2017). In-situ Synthesis of WC/TaC Reinforced Nickel-Based Composite Alloy Coating by Laser Cladding. *Rare Metal Materials and Engineering, 46*(11), 3176–3181.

[13]. Kumar, S., Mondal, S., Kumar, A., Ranjan, A., & Prasad, N. (2017). Chemical Vapor Deposition of TaC/SiC on Graphite Tube and Its Ablation and Microstructure Studies. *Coatings, 7*, 1-12.

[14]. Nakamura, D., Kimura, T., Narita, T., Suzumura, A., Kimoto, T., & Nakashima, K. (2017). TaC-coated graphite prepared via a wet ceramic process: Application to CVD susceptors for epitaxial growth of wide-bandgap semiconductors. *Journal of Crystal Growth, 478*, 163–173.

[15]. Behera, N., Kumar, A., Chaudhary, S., & Pandya, D. K. (2017). Two magnon scattering and anti-damping behavior in a two-dimensional epitaxial TiN/Py(tPy)/β-Ta(tTa) system. *RSC Advances, 7*(14), 8106–8117.

[16]. Kim, D., Jeong, S.M., Yoon, S.G., Woo, C.H., Kim, J. I., Lee, H. G., Park, J. Y.,& Kim, W. J, (2016). Chemical Vapor Deposition of Tantalum Carbide from $TaCl_5$-C_3H_6-Ar-H_2 System. *Journal of the Korean Ceramic Society*, 53, 597-603.

[17]. Tanwar, D., Gohar, S. K., Ram Sankar, P., (2018). Corrosion Inhibition of Mild Steel by Benzotriazole in 1M and 2M Sulfuric Acid Solution. *International Journal of Theoretical & Applied Sciences, 10*, 140-145.